Steady-State Analysis and Comparison of SSFB, SDFB and DSFB MMC-based STATCOM

Mohamed Moez BELHAOUANE[1], Pierre VERMEERCH[1], François GRUSON[1], Pierre RAULT[2], Sébastien DENNETIERE[2], Xavier GUILLAUD[1]

[1]Univ. Lille, Arts et Métiers Institute of Technology, Centrale Lille, Junia, ULR 2697 - L2EP, F-59000 Lille, France.

E-Mail : mohamed-moez.belhaouane, pierre.vermeerch, xavier.guillaud @centralelille.fr, francois.gruson@ensam.eu

[2] RTE (Réseau de Transport d'Electricite), Research and Development Department of RTE, 92073, Paris La Défense, France.

E-Mail : pierre.rault, sebastien.dennetiere@rte-france.com

Acknowledgements

This research work has been supported by RTE, the French TSO (Transmission System Operator).

Keywords

« Static Synchronous Compensator (STATCOM) » « Modular Multilevel Converters (MMC)» « Double-Star Full Bridge » « Single-Star Full Bridge » « Single-Delta Full Bridge » « Energy requirement » « Losses estimation ».

Abstract

This work focuses on the steady-state analysis of three types of MMC based STATCOM. For a given STATCOM rating, Double-Star Full Bridge, Single-Star Full Bridge and Single-Delta Full Bridge have been compared in terms of design and losses. In this approach, the number of submodules is chosen according to the voltage and current ratings of semiconductor devices while the submodule capacitor value is obtained by following an energy storage criterion to maintain the submodule voltages within an acceptable voltage range.

Introduction

STATCOM are commonly considered for voltage regulation and control, reactive power compensation, improvement of steady state power transfer capacity, improvement of power quality such as flicker and harmonics, improvement of transient stability margin, damping power system oscillations and sub-synchronous oscillations, balancing loads of individual phases and eventually application including storage [1]. More recently, the massive penetration of renewable energy sources has increased the interest in HV STATCOM applications to strengthen the grid. The STATCOM-MMC family is usually classified into four topologies [2]:Single-Star Full Bridge (SSFB), Single-Delta Full Bridge (SDFB), Double-Star Full-Bridge (DSFB) and Double-Star Half-Bridge (DSHB). The single-star full-bridge and the single-delta full-bridge (FB) are based on three strings of multiple FB cells with star and delta connection, respectively. The double Star Full-Bridge (FB) and Half-Bridge (HB) topologies are based on two sets of star-configured converters in which the AC side of multiple FB and HB cells are cascaded to constitute each arm [3]. This topology is the same as an AC/DC converter station. Usually, this topology is seen in literature as unsuitable topology due its higher number of power devices. However, for STATCOM application, it seems to be interesting to investigate this structure compared to DSHB [4]. In terms of commercial application, some topologies have been implemented. For instance, the

SDFB topology has been adopted as STATCOM station and energy storage interface for an already operational project as illustrated in [5].

Nevertheless, few works in literature present an in-depth steady-state comparison study between the different topologies, presented above, for STATCOM application. For instance, in [2], only the difference in terms of the number of SMs has been evaluated for different topologies. In [6] a comparison of the two double star topologies, such as DSFB and DSHB, has been proposed. These topologies are compared in terms of steady-state operation, power losses and costs. The reference [7] compares the losses and topology cost of SDFB and DSHB topologies for STATCOM application based on a 100 MVA case study. In addition, regarding the converter losses, only the contribution of power semiconductor devices has been considered. In fact, few comparison studies related with the energy storage requirement ensuring a reliable operation of the topology are proposed in literature. In this sense, the authors in [8] propose some comparisons, which are supported by analytical results regarding minimum effective DC-bus voltage, number of SMs, current rating, energy storage requirements and operation during unbalanced conditions. However, only DSHB and SDFB topologies have been investigated for a 15 MVA MMC-STATCOM. Therefore, there is a lack of a more global comparative study between the main MMC topologies, about the main design criteria for a STATCOM application.

This paper aimed to provide a comprehensive approach on the design of MMC-STATCOM for high voltage application for different topologies:

- **(i)** Proposition of steady-state analysis methodology allowing the design of SMs number per arm , the energy storage requirements and total losses including power electronic and passive high voltage equipment losses.
- **(ii)** Comparison of the three topologies in terms of arm design, storage energy requirments and semiconductor losses based on the elaborated criteria in **(i).** The comparison of the necessary components gives an insight of the total cost associated with each topology.
- **(iii)** Identification of the most efficient and reliable MMC-STATCOM topology that meets the defined criteria in the proposed study.

It can be demonstrated that the DSHB would induce an important energy storage requirement compared with the three other topologies [8]. So only SSFB, SDFB and DSFB will be studied in this paper.

The paper is outlined as follows. The configuration of the three main MMC-STATCOM topologies are detailed in section 2. The section 3 presents the steady-state analysis based on single star full-bridge configuration, considered as reference topology. The proposed methodology involves submodules number calculation and stored energy requirement per arm as well as total losses estimation. The expansion of the proposed design methodology on SDFB and DSFB Topologies is proposed in section 4. A comparative study between the studied configurations (i.e., SSFB, SDFB and DSFB) is performed to assess the steady-state performances of MMC-STATCOM topologies. The last section summarizes the main conclusions drawn from the analysis, showing the best topology of MMC-STATCOM based on the proposed criteria through this study.

STATCOM Topologies Description

As mentioned above, only the topologies with submodules (SM) in full-bridge configuration are considered. The circuit diagrams of the three main topologies are highlighted in Fig. 1. As shown, the DSFB topology presents 6 arms (Fig. 1c), while the SSFB and SDFB topologies presents 3 arms (Fig. 1a, Fig. 1b respectively). Each arm consisting of an inductor L_{arm}, an internal resistance R_{arm} and N-full-bridge cell capacitance C_{SM}. The converter is connected to the AC grid through the three-phase transformer connection impedance which is characterized by its transformation ratio and its leakage inductance (L_f, R_f). The grid side is modelled as a voltage source $v_{gj,j=a,b,c}$, with $i_{gj,j=a,b,c}$ are the three-phase grid current. The modulated voltages are designed by $v_{mj,j=a,b,c}$ (resp. $u_{mj,j=ab,bc,ca}$). As mentioned above, the SMs in SSFB, SDFB and DSFB topologies are of full bridge type, since both positive and negative voltages are required for the operation of the converter.

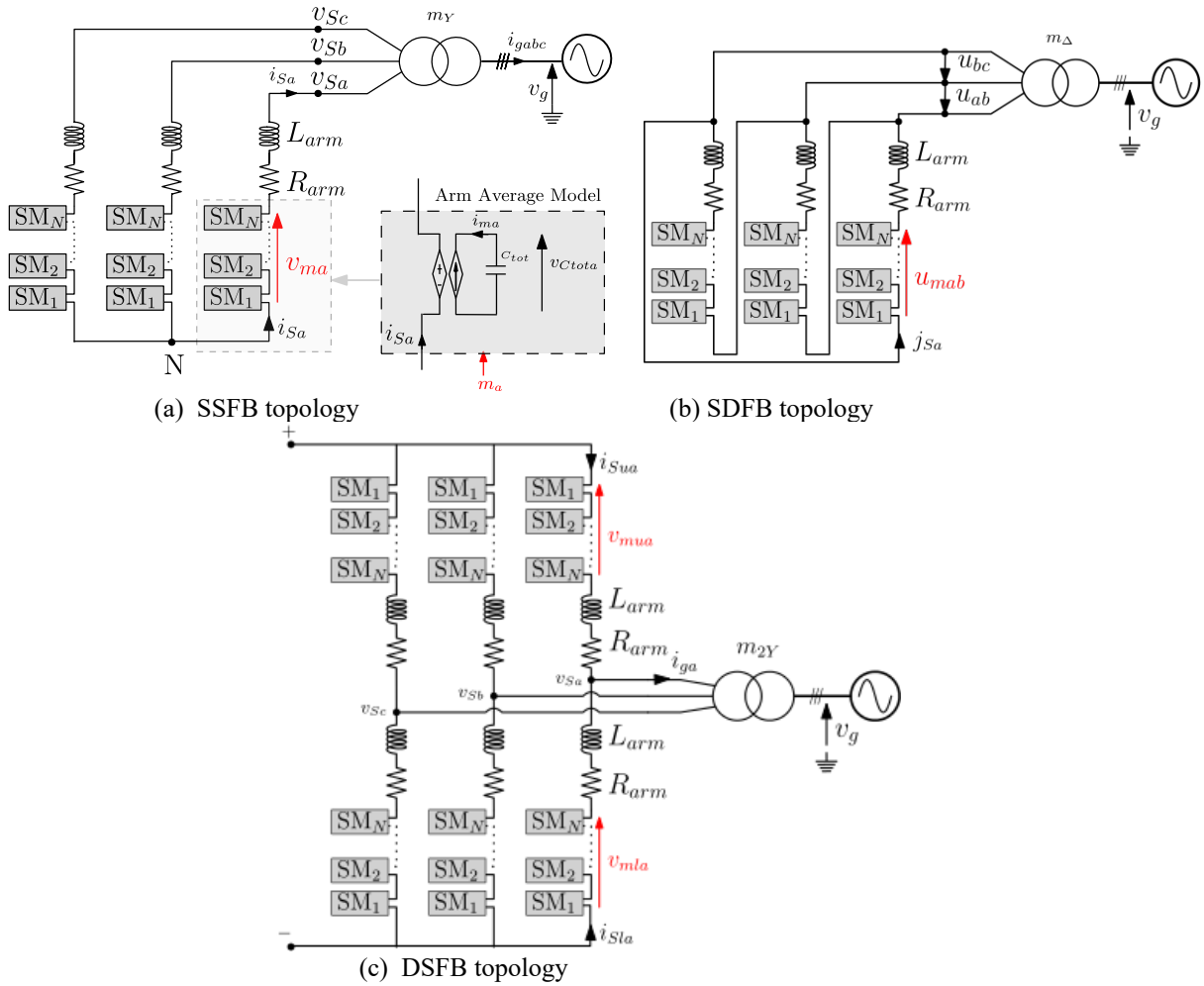

(a) SSFB topology (b) SDFB topology

(c) DSFB topology

Fig. 1: Classification of studied topologies

In addition, thanks to degrees of freedom, the Zero-sequence is considered to improve the design, a voltage v_{NO} is considered for star topology while a current i_0 for delta topology.

STATCOM Design: Example of Single-Star Full Bridge (SSFB) Topology

The same methodology is applicable for the three different topologies; however, it is only detailed on the SSFB configuration. First, the nominal arm current is obtained from the rating of power electronic devices which are connected in series. For instance, considering a 3300V-1500A, single switch IGBT - *Infineon FZ 1500R33HL3* [9], the arm current is defined as follow:

$$I_{SY} = I_{SY_{nom}} = \frac{1500}{\sqrt{2}} = 1061 \text{ Arms} \tag{1}$$

Considering a 300 MVA STATCOM connected to a 400kV grid, the nominal grid current is defined as follow:

$$I_{g_{nom}} = \frac{S_{nom}}{\sqrt{3}\times U_{nom}} = \frac{300MVA}{\sqrt{3}\times 400kV} = 433 \text{ Arms} \tag{2}$$

The interface transformer ratio is defined according to the ratio between the grid current and the valve current:

$$m_Y = \frac{I_{gnom}}{I_{SY}} = \frac{433}{1061} = 0.408 \tag{3}$$

The valve nominal voltage line to line is directly derived from the transformer ratio:

$$U_S = m_Y U_g = 0.408 \times 400 = \ 163\ kV \tag{4}$$

A. *Number of submodules (N_{SM})*

To determine the number of SMs per arm, a simplified phasor diagram (c.f., Fig. 2) can be used in per-unit system to determine the peak value of the modulated voltage that should be generated by the arm of SMs.

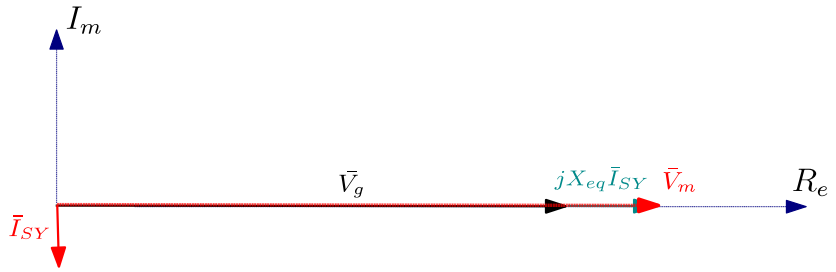

Fig. 2: Simplified phasor diagram by neglecting the resistive components

Therefore, depending on the topology, the operating point and the equivalent connection impedance (transformer leakage impedance and L_{arm}), the minimal number of SM (N_{SM}) can be expressed through the following equation when the STATCOM is injected the nominal power to the grid:

$$N_{SM} = \left\lceil \frac{\sqrt{2}}{V_{SM}} \left(\frac{m_Y U_g}{\sqrt{3}} + X_{eq} I_{SY_{nom}} \right) \right\rceil = \left\lceil \frac{\sqrt{2}}{1600V} \left(\frac{163kV}{\sqrt{3}} + 0.3 \times \frac{163^2}{300} \times 1061 \right) \right\rceil \approx 110 \tag{5}$$

where $X_{eq} = X_{arm} + X_T$ ($i.e., X_{arm}$=0.15 p.u and X_T =0.15 p.u) is the equivalent AC side impedance and V_{SM} is the submodule voltage (e.g., $V_{SM} = 1600V$). Thus, according to (5), the number of submodules is equal to $N_{SM} \sim 110$. In order to reduce the number of SM, a zero-sequence voltage injection (ZSVI) based on the following injection scheme [10] can be performed as

$$v_{NO} = -\frac{\max[v_{mj}]+\min[v_{mj}]}{2} \tag{6}$$

From (6), it results in a triangular waveform, naturally synchronous with STATCOM voltage v_S and its magnitude equals to $\frac{1}{4}$ of $\hat{V}_S$ [10]. Therefore, ZSVI allows the reduction of the required N_{SM} per arm by almost 15% for SSFB. Therefore, in our example the number of SMs can be reduced to 94.

B. *Estimation of the stored energy requirement*

The second step is to design the SM capacitors. The need of the internal energy storage depends on the acceptable SM capacitor voltage variation, caused by current oscillation over one network period. By assuming a perfect SM voltage balancing, it has been depicted in previous works [11], that an arm of SMs can be modelled using an average model that consists in an equivalent DC/DC converter. A more usual metrics to characterize the storage of energy is the constant H_c which corresponds the total energy divided by the nominal power [12].

$$H_c = \frac{\frac{1}{2} N_{arm}\, C_{tot}\, v_{Ctot}^2}{S_n} \tag{7}$$

with N_{arm} the number of arms, C_{tot} the total SMs capacitance (c.f. Arm Average Model in Fig. 1) and S_n the rated power. To estimate H_c, two methods have been proposed in literature [13]. The method developed in [14] has been used in this work. It is based on the limitation of the peak-to-peak voltage ripple defined as $\Delta v_{Ctot} = \hat{v}_{Ctot} - \check{v}_{Ctot}$, where $\hat{v}_{Ctot}$ and $\check{v}_{Ctot}$ are corresponding to the maximum and minimum voltages, respectively. The oscillations voltage ripple in the capacitors come from the

waveform of the instantaneous power ($p_{C_{tot}}$). This power is calculated for the nominal value of the reactive power from the instantaneous steady state value of the voltage v_m and the arm current i_{arm}.

$$v_m = \left(\frac{m_Y U_g}{\sqrt{3}} + X_{eq} I_{S_Y}\right)\sqrt{2}\, sin(\omega t) \tag{8}$$

$$i_{arm} = I_{S_Y}\sqrt{2}\sin\left(\omega t \pm \frac{\pi}{2}\right) = \frac{I_g}{m_Y}\sqrt{2}\sin\left(\omega t \pm \frac{\pi}{2}\right) = \frac{Q_n}{\sqrt{3}U_g m_Y}\sqrt{2}\sin\left(\omega t \pm \frac{\pi}{2}\right) \tag{9}$$

Based on (8) and (9), the instantaneous power expression in per-unit with $Q_n = S_n$ can be expressed as:

$$p_{Ctot\,pu} = \left(\frac{1}{3} + \frac{X_{eq}^{pu}}{3}\right)\cos\left(2\omega t \pm \frac{\pi}{2}\right) \tag{10}$$

By integrating (10), the peak-to-peak energy fluctuation Δw_{Ctot} is derived as:

$$\Delta w_{Ctot} = \frac{1}{\omega}\left(\frac{1}{3} + \frac{X_{eq}^{pu}}{3}\right) \tag{11}$$

If the average value of v_{Ctot} is assumed to be maintained around its nominal value V_{Ctot0}, then the total capacitor voltage can be expressed as:

$$v_{Ctot} = V_{Ctot0}\left(1 + \delta_{v_{Ctot}}\right) \tag{12}$$

where $\delta_{v_{Ctot}}$ is the voltage oscillation introduced by the AC component in the arm quantities. This oscillation is assumed to be evenly distributed around V_{Ctot0}. So, the peak-to-peak energy fluctuation can be express depending to the maximum and minimum energy variation as $\Delta w_{Ctot} = \hat{\delta} w_{Ctot} - \check{\delta} w_{Ctot}$, with:

$$\begin{cases} \hat{\delta} w_{Ctot} = \frac{1}{2} C_{tot} V_{Ctot0}^2 \left(1 + \delta_{v_{Ctot}}\right)^2 \\ \check{\delta} w_{Ctot} = \frac{1}{2} C_{tot} V_{Ctot0}^2 \left(1 - \delta_{v_{Ctot}}\right)^2 \end{cases} \tag{13}$$

Then, we obtain:

$$\Delta w_{Ctot} = \frac{1}{2} C_{tot} V_{Ctot0}^2 \left(1 + 2\delta_{v_{Ctot}} + \delta_{v_{Ctot}}^2 - 1 + 2\delta_{v_{Ctot}} - \delta_{v_{Ctot}}^2\right) = \frac{1}{2} C_{tot} V_{Ctot0}^2 4\delta_{v_{Ctot}} \tag{13}$$

According to (7) for STATCOM application (i.e., $S_n = Q_n$), it is possible to substitute the expression of C_{tot} in (14), to obtain:

$$\Delta w_{Ctot} = \frac{4\, H_c Q_n \delta_{v_{Ctot}}}{N_{arm}} = \frac{2\, H_c Q_n \Delta v_{Ctot}}{N_{arm}} \tag{15}$$

Thus, the value of H_c which guarantee the peak-to-peak voltage ripple Δv_{Ctot} is defined as:

$$H_c = \frac{N_{arm}\, \Delta w_{Ctot}}{2 Q_n\, \Delta v_{Ctot}} \tag{14}$$

with N_{arm}= 3 for SSFB. From (16) and by considering X_{eq}^{pu} equals to 0.3 pu and $\Delta v_{Ctot} = 0.2\ pu$, we obtain:

$$H_c = 10.5\ \frac{\text{kJ}}{\text{MVA}} \tag{15}$$

In order to validate the stored energy requirement for SSFB configuration, obtained in (17), time-domain simulation based on Arm Average Model (see Fig. 1a) has been performed for maximal reactive power operating point. It can be checked that the peak-to-peak voltage ripple is equal to $\Delta v_{Ctot} = \hat{v}_{Ctot} - \check{v}_{Ctot} = 0.2\ pu$ as shown in Fig. 3.

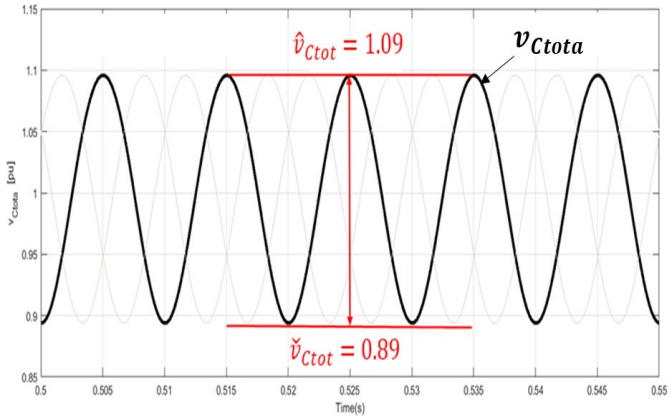

Fig. 3: H_C validation based on steady state time-domain response of v_{Ctota}

For simplicity of the presentation, the zero-sequence voltage has not considered in this steady-state modeling, but the methodology can be extended with this zero-sequence injection.

C. Semi-conductor loss estimation

The evaluation of losses in the MMC has been widely covered in the literature according to different methods, e.g., in [15]. In this study, power losses estimation relies on hybrid method combining the steady state analytical model and time domain simulation as depicted in Fig. 4, to get a fast estimation. The proposed semi-conductor loss estimation method is based on the previous work detailed in [11], extended to full-bridge SM configuration. From the sinusoidal waveform of the modulated voltage (v_m) and the arm current (i_{arm}), it is possible to simulate for an arm, the Capacitor-Balancing Algorithm (CBA) associated with the low level control, as shown in Fig. 4.

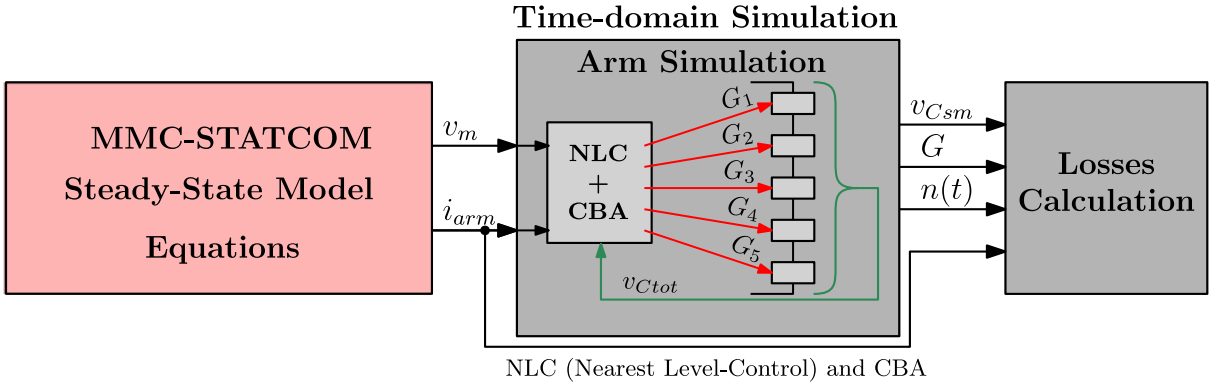

Fig. 4: Generic flow-chart of losses estimation method

For this study, the used CBA is based on the algorithm detailed in [11]. According to an execution time of 10 μs, the maximal voltage variation recorded is 320V between the most and least charged SM capacitors (i.e., 0.2 pu). This CBA execution time allows maintaining the switching frequencies around $\overline{f_{sw}} = 180\ Hz$.

The proposed method avoids performing an EMT simulation of the complete system, therefore reduces the computation effort and save time. Fig. 5a, shows the waveforms of a single-phase modulated voltage v_m and arm current i_{arm} in case of an injection of third harmonic. The SM capacitor voltages shown in Fig. 5b are obtained by the block which includes module selection and valve model. This block also provides the relevant inputs to the valve loss estimation which corresponds to SMs capacitors voltages, gate signals, and the arm currents.

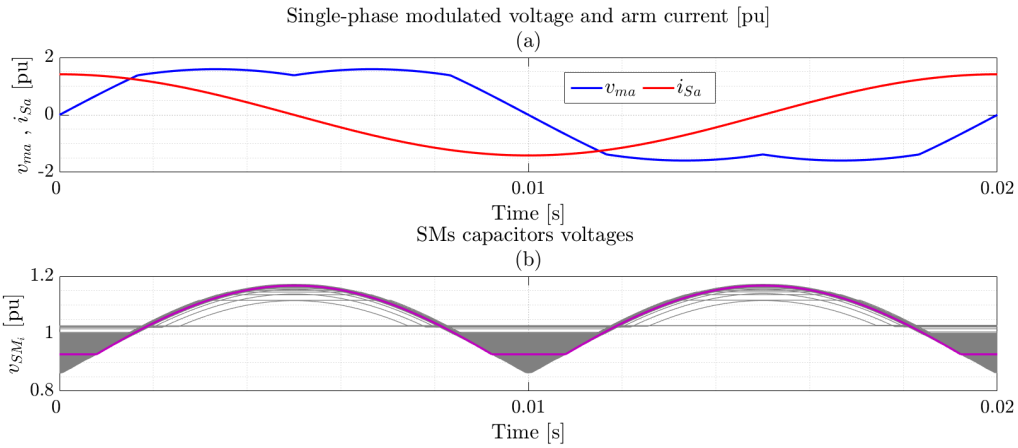

Fig. 5: Arm Voltage and current waveforms, and submodule voltages for phase (a)

As mentioned above, this algorithm discussed in [16], has been performed for HB-SM and adapted in this work to FB-SM, where the key elements are recalled in the following lines. As explained in [11], the semiconductor losses in the MMC can be derived into conduction and switching losses. From the datasheets of power electronic components (c.f., Infineon FZ 1500R33HL3), the VI static characteristics of IGBT and diode are approximated by polynomial functions of third order. In fact, the polynomial function corresponding to the on-state voltage characteristics versus the current for both IGBT and diode, denoted as $V_{CE(sat)}(i_{arm}, T_j)$ and $V_D(i_{arm}, T_j)$, respectively. In this work, for simplicity, the junction temperature T_j is kept constant equal to 125°C. In real life project, the temperature can be adapted to the operating point to get more accurate results. Thus, the conduction losses in the semiconductors of a given submodule can be calculated as the product of the arm current and its voltage drop as defined in [16]. Therefore, diode and IGBTs conduction losses of each FB-SMs are evaluated according to (18) and (19), respectively.

$$p_{c,Diodes\ D1\to D4}(t) = f_{D1\to D4}.\, i_{arm}.\, V_D(i_{arm}, T_j) \tag{16}$$

$$p_{c,IGBT\ T1\to T4}(t) = f_{T1\to T4}.\, i_{arm}.\, V_{CE(sat)}(i_{arm}, T_j) \tag{19}$$

where $f_{D1\to 4}$ and $f_{T1\to 4}$ are the Boolean functions, when the assigned valued is equal to one means that the current is following through the respective element and zero otherwise. The average conduction losses in the arm is calculated by integrating (18)-(19) over a fundamental period T using discrete-time integration.

Then, the switching losses in FB-SMs supposed to calculate energy which is lost at each commutation for IGBT (E_{ON} and E_{OFF}) and diode (E_{rec}). These energies are approximated by a polynomial description thanks to the switching energy characteristics of the module given from datasheets as curves in function of arm current (for a given T_j). So, based on the polynomial description of E_{ON}, E_{OFF} and E_{rec}, the energy lost at each commutation are expressed by the following equations.

$$IGBT_{Turn-ON} \to E_{ON}(i_{arm}, T_j)\frac{v_{Csmi}}{V_{CC}} \tag{20}$$

$$IGBT_{Turn-OFF} \to E_{OFF}(i_{arm}, T_j)\frac{v_{Csmi}}{V_{CC}} \tag{21}$$

$$Diode_{Turn-OFF} \to E_{rec}(i_{arm}, T_j)\frac{v_{Csmi}}{V_{CC}} \tag{22}$$

where v_{Csmi} is the submodule capacitor voltage value at a switching instant. V_{CC} is the voltage used by manufacturers to determine the energy lost during the switching (e.g., $V_{CC} = 1800\ V$). Then, the total switching losses at each commutation instant can be obtained, and the results are summed up and averaged over a fundamental period T.

The losses of passive element such as arm reactor and transformer are not presented in this paper but are added to total loss estimation.

The obtained power losses result according to the reactive power variation are given in Fig. 6, where the impact of ZSVI has been investigated. From Fig. 6a, in both capacitive and inductive modes, the SSFB without ZSVI exhibits almost similar levels of losses. AC high voltage Transformer with 99.75% of efficiency and 0.05% of winding resistances lead to 0.75 MW as losses in the transformer, below conduction losses at rated reactive power. The losses within the arm for a ratio $\frac{X}{R} \approx 200$ gives $P_{Rarm} \sim 0.23\ MW$, which are slightly below the switching losses. In fact, the switching losses in IGBTs are relatively low (i.e., $P_{SW} \sim 0.28\ MW$) compared to the total losses inside the converter. A second test on power losses estimation has been performed when using ZSVI as displayed in Fig. 6b. It is recalled that the zero-sequence voltage injection is based on (6) according to $\frac{1}{4}$ of maximal STATCOM voltage $\hat{V}_S$ as magnitude of v_{NO}. The details with respect to power losses based on ZSVI are highlighted through Table I. As it can be observed, the ZSVI allows reducing slightly the losses (mainly the conduction losses). Based on ZSVI, the total losses minimization is around $200\ kW$.

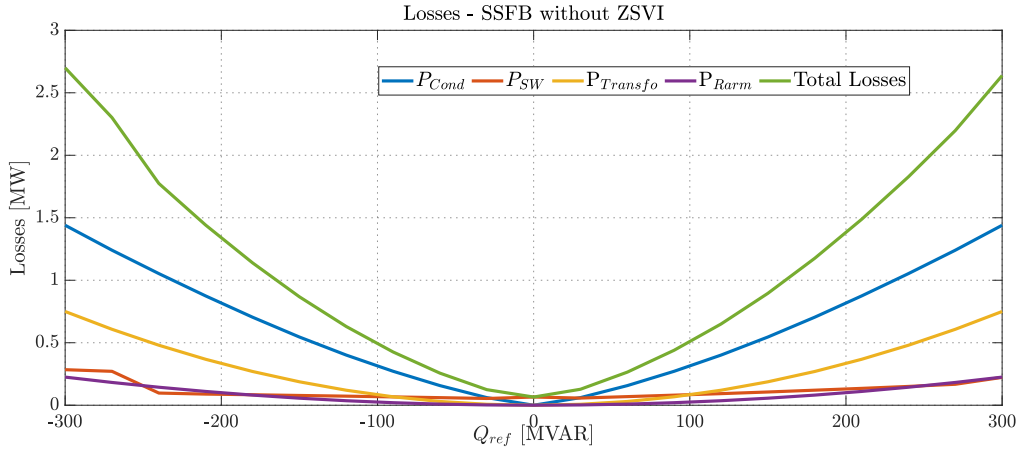

(a)

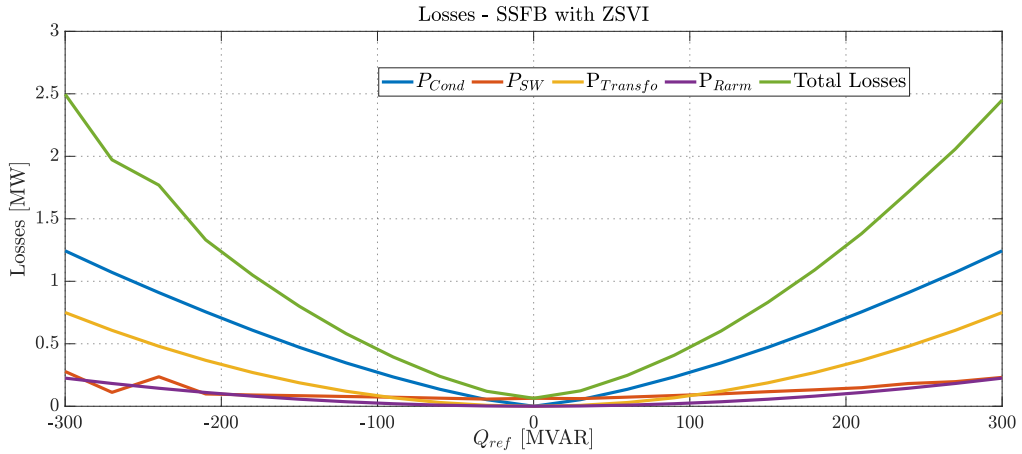

(b)

Fig. 6: Power losses in SSFB respect to reactive power reference Q_{ref} – (a): without ZSVI, (b): with ZSVI

Table I: Estimation of losses based on MMC-SSFB with ZSVI

	Absorption	Injection
Conduction Losses [MW]	**1.24**	**1.24**
Switching Losses [MW]	**0.28**	**0.24**
Transformer Losses [MW]	**0.75**	**0.75**
Arm Losses [MW]	**0.23**	**0.24**
Total Losses [MW]	**2.50**	**2.45**

Application of the proposed methodology to SDFB and DSFB Topologies and Comparative Results

The proposed methodology for the design of STATCOM topologies has also been applied to MMC-SDFB and MMC-DSFB configurations. To achieve a fair comparison, the same transistor is used for each topology. To obtain the same RMS current in the transistor, the transformer ratio m must be adjusted as shown in Table II.

Table II: Comparative results for a single arm in terms of $\boldsymbol{m}$, $\boldsymbol{N_{SM}}$ and $\boldsymbol{H_c}$

	MMC-SSFB	**MMC-SDFB**	**MMC-DSFB**
$\boldsymbol{m}$	0.408	0.235	0.204
$\boldsymbol{N_{SM}}$	110	110	55
$\boldsymbol{H_c(\frac{kJ}{MVA})}$	10.5	10.5	10.5

From Table II, it can be displayed that the number of submodules per arm (N_{SM}) is the same for SSFB and SDFB. However, N_{SM} is twice less for the DSFB but since there are twice more arm, the total number of submodules is the same. When using the ZSVI, it is possible to decrease N_{SM} by 15% for SSFB and DSFB. On the SDFB topology, the zero-sequence current injection (ZSCI) has been assessed with a magnitude of $\frac{1}{6}$ of $\hat{I}_S$. It has been observed that ZSCI does not have a significant impact on N_{SM} for the delta configuration. In addition, the proposed design method of H_c has been performed also on the two other topologies. As displayed in Table II, the same value for the H_c index is obtained for each topology.

In terms of total losses, Fig. 7a shows quite similar results between the three topologies where no zero-sequence injection has been considered. Fig. 7b depicts the total losses by considering the ZSVI and ZSCI. It has been established that DSFB is more efficient compared to SSFB and SDFB. Indeed, a noticeable total loss reduction is observed for double-star topology respecting the total losses within the structure. Such difference involves around 16% of reduction (i.e., $\Delta P_{tot} \sim 410\ kW$) compared to SSFB and 19% (i.e., $\Delta P_{tot} \sim 503\ kW$) compared to SDFB.

Finally, from the proposed study, it is possible to conclude that DSFB is the most appropriate topology since it is more efficient while allowing losses minimization with ZSVI compared to SSFB and SDFB. In addition, using ZSVI, it is possible to decrease the total number of submodules by 15% and therefore minimize the cost of double-star topology.

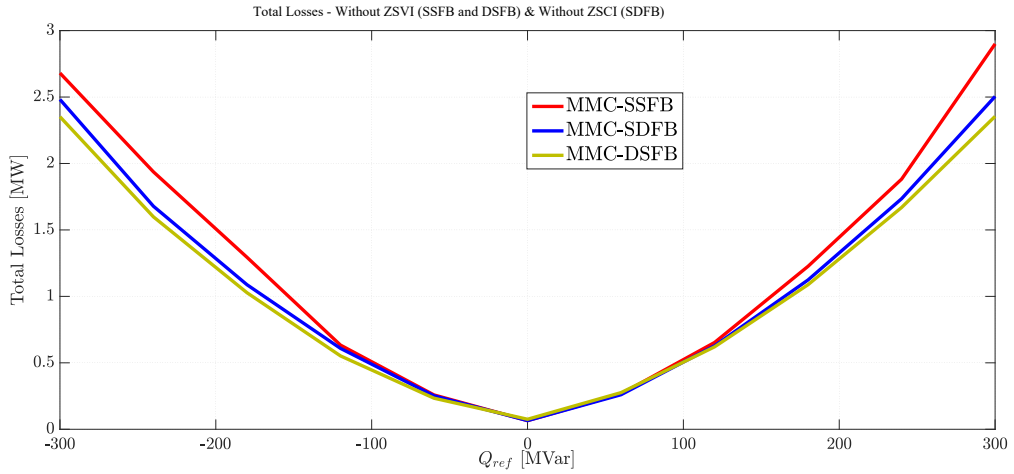

(a)

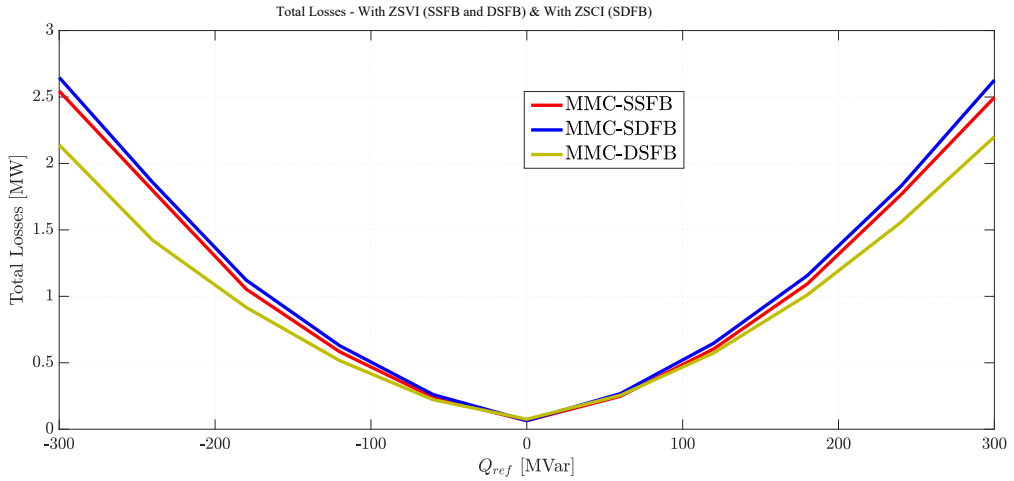

(b)

Fig. 7: Total losses estimation comparison respect to a variation of Q_{ref} – (a): without ZSI, (b): with ZSI

Conclusion

This paper gives a comprehensive steady-state analysis of the MMC-SSFB, MMC-SDFB and MMC-DSFB configurations in their application as STATCOM in transmission system. The proposed study focuses mainly on the stored energy requirements, submodules number design and total losses estimation to assess the design cost of each topology. A precise methodology based on a steady state analytical model of MMC-STATCOM has been performed. An in-depth comparison between the studied topologies is carried out to provide quantitative criteria to choose the MMC topology for STATCOM application. In addition, the impact of zero sequence voltage and current injection on the topology design has been discussed. The key points can be given: In terms of power losses, the DSFB is the best topology compared to SSFB and SDFB, especially when using ZSVI. A total loss reduction around 16% and 19% compared to SSFB and SDFB, respectively. The use of ZSVI induces also a 15% decrease of N_{SM} (i.e., the number of switches) in both single- and double-star topologies whereas the ZSCI has nearly no impact in case of SDFB. Then, it can be concluded that the double-star full bridge is the most appropriate topology for the MMC-STATCOM that meets the defined criteria in the proposed study.

As future works, the comparison between the investigated topologies may spread in dynamics to assess the dynamic performances under normal and distorted AC grid conditions. Furthermore, it seems interesting to extend the proposed design methodology for unbalanced and fault grid conditions using a steady state model of MMC-STATCOM based on the negative sequence components.

References

[1] "STATIC SYNCHRONOUS COMPENSATOR (STATCOM)", CIGRE Technical Brochure 144, Working Group 14.19, 2000.

[2] H. Akagi, "Classification, terminology, and application of the modular multilevel cascade converter (MMCC)", *IEEE Trans. Power Electronics*, vol. 26, n°.11, p. 3119–3130, 2011.

[3] S.G. Mian, P.D. Judge, A. Junyent-Ferr and T. Green, "A Delta-Connected Modular Multilevel STATCOM with Partially-Rated Energy Storage for Provision of Ancillary Services", *IEEE Transactions on Power Delivery*, vol. 36, n°15, pp. 2893-2903, 2021.

[4] E. Behrouzian, M. Bongiorno and H. Z. De La Parra, "Investigation of negative sequence injection capability in H-bridge multilevel STATCOM", *16th Conference on Power Electronics and Applications*, pp. 1-10, 2014.

[5] E. Spahic, C. P. Susai Sakkanna Reddy, M. Pieschel, and R. Alvarez, "Multilevel STATCOM with power intensive energy storage for dynamic grid stability - frequency and voltage support", *IEEE Electrical Power and Energy Conference (EPEC)*, pp. 73-80, 2015, London, UK.

[6] R. O. d. Sousa, D. d. C. Mendonça, W. C. S. Amorim, A. F. Cupertino, H. A. Pereira and R. Teodorescu, "Comparison of Double Star Topologies of Modular Multilevel Converters in STATCOM Application", *13th IEEE International Conference on Industry Applications,* pp. 622-629, 2018.

[7] H. A G. Tsolaridis, H. A. Pereira, A. F. Cupertino, R. Teodorescu, and M. Bongiorno, "Losses and cost comparison of DS-HB and DS-FB M based large utility grade STATCOM", *in 16th EEEI Conference*, pp. 1-6, June 2016.

[8] A. F. Cupertino, J. V. M. Farias, H. A. Pereira, S. I. Seleme and R. Teodorescu, "Comparison of DSCC and SDBC Modular Multilevel Converters for STATCOM Application During Negative Sequence Compensation", *in IEEE Transactions on Industrial Electronics*, vol. 66, n°13, pp. 2302-2312, March 2019.

[9] www.infineon.com/cms/en/product/power/igbt/igbt-modules/fz1500r33he3/

[10] O. Ojo, "The generalized discontinuous PWM scheme for three-phase voltage source inverters", *IEEE Transactions on Industrial Electronics*, vol. 51, n°16, pp. 1280-1289, 2004.

[11] P. Vermeersch, "Contribution to the Design and Control of the Extended Overlap-Alternate Arm Converter", *PhD. Thesis*, Ecole Centrale de Lille, L2EP, September 2021.

[12] H. Saad, "Modélisation et simulation d'une liaison HVDC de type VSC-MMC ", *PhD Thesis*, Université de Montréal, 2015.

[13] S. Heinig, K. Ilves, S. Norrga, and H. P. Nee, "On energy storage requirements in alternate arm converters and modular multilevel converters", *in Proceedings of the 18th European Conference on Power Electronics and Applications, EPE 2016 ECCE Europe*, 2016.

[14] M. M. Merlin and T. C. Green, "Cell capacitor sizing in multilevel converters: Cases of the modular multilevel converter and alternate arm converter", *IET Power Electronics,,* vol. 8, n°13, pp. 350-360, 2015.

[15] C. Oates and C. Davison, "A comparison of two methods of estimating losses in the modular multi-level converter", *14th European Conference on Power Electronics and Applications*, EPE'11, pp. 1–10, August 2011.

[16] J. Freytes, F. Gruson, P. Delarue, F. Colas, X. Guillaud, "Losses Estimation Method by Simulation for the Modular Multilevel Converter", *EPEC conference*, London, Ontario, October 2015.

[17] A. Hassanpoor, L. Angquist, S. Norrga, K. Ilves and H. Nee, "Tolerance Band Modulation Methods for Modular Multilevel Converters," *in IEEE Transactions on Power Electronics*, vol. 30, no. 1, pp. 311-326, Jan. 2015.

[18] "Power losses in voltage sourced converter (VSC) valves for high-voltage direct current (HVDC) systems – Part 2: Modular multilevel converters", *IEC 62751-2*, August 2019.